ISCI, Volume *16*

Supplemental Information

Electrical Polarization Enables Integrative Quality Control during Bacterial Differentiation into Spores

Teja Sirec, Jonatan M. Benarroch, Pauline Buffard, Jordi Garcia-Ojalvo, and Munehiro Asally

Supplementary figures and legends

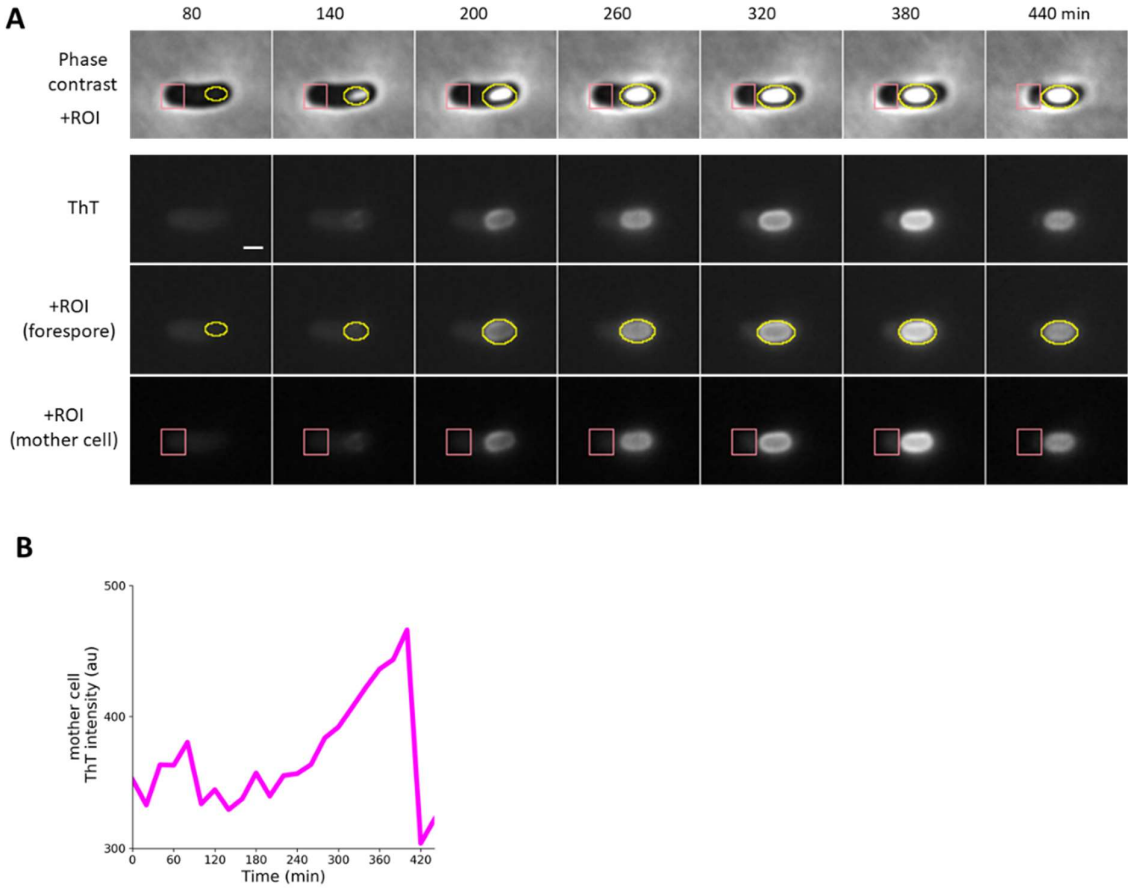

Figure S1. Single-cell image analysis, Related to Figure 1
A) Yellow and Magenta indicate the ROIs (region of interest) used for the intensity measurement on spore and in mother cell, respectively. Images correspond to Figure 1. **B)** ThT intensity over time measured for the mother-cell region (magenta square in panel A).

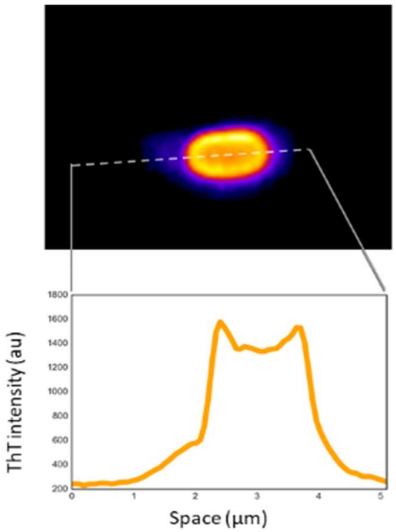

Figure S2. ThT accumulates on the periphery of forespores, Related to Figure 1
ThT fluorescence intensity over the space along the dashed line shown in the image.

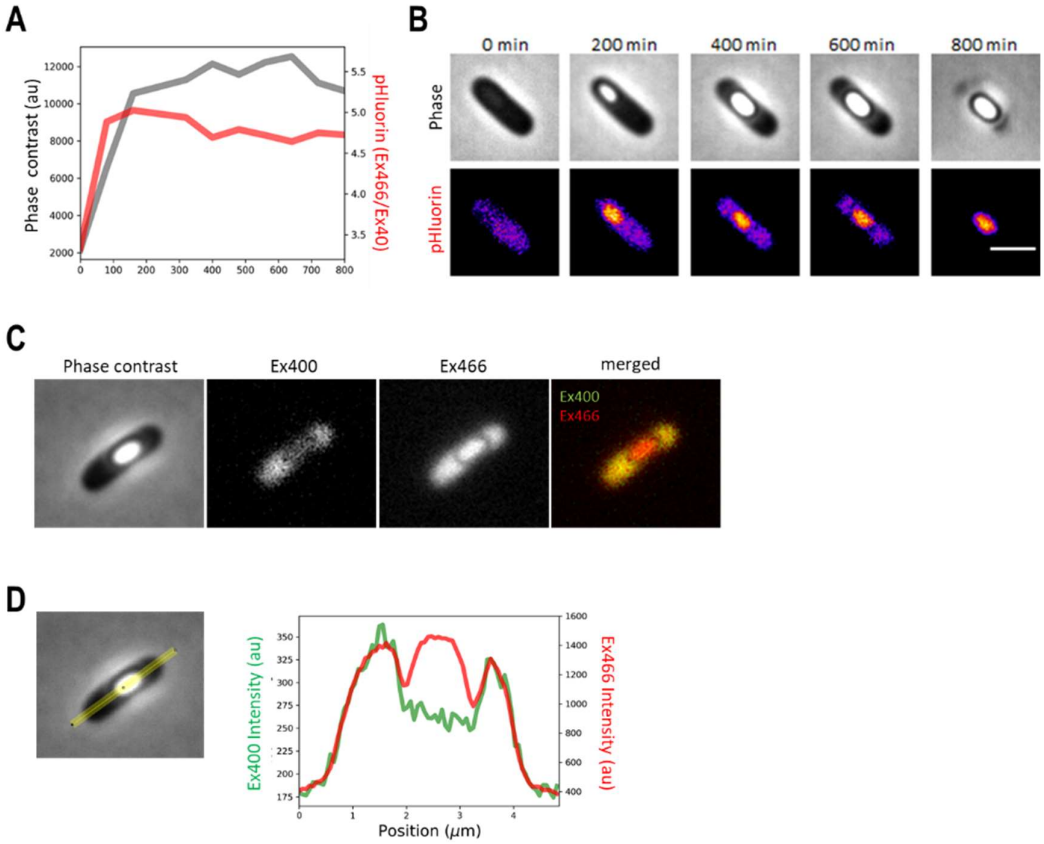

Figure S3. pH dynamics during sporulation, Related to Figure 1

A) Time series of forespore/endospore intensities of phase contrast channel in grey and pHluorin in red (Ex466/Ex400 ratio) in wild type strain. Time series shows a steep acidification of forespore cytoplasm coinciding with the occurrence of phase-bright spore. Time series is representative from five independent experiments. We emphasize that the plateau signal after initial increase does not mean pH is stable. This is because pH may be out of the pHluorin dynamic range. **B)** Film-strip images showing the phase-contrast channel (upper) and pHluorin Ex466/Ex400 ratio (lower). Scale bar, 2 μm. **C)** microscopy images of phase-contrast, Ex400, Ex466 channels and merged image of Ex400 and Ex466. pHluorin is likely excluded from the forespore periphery due to the assembly of coat layers. **D)** Ex400 and Ex466 fluorescence signals from pHluorin were plotted along the yellow line shown.

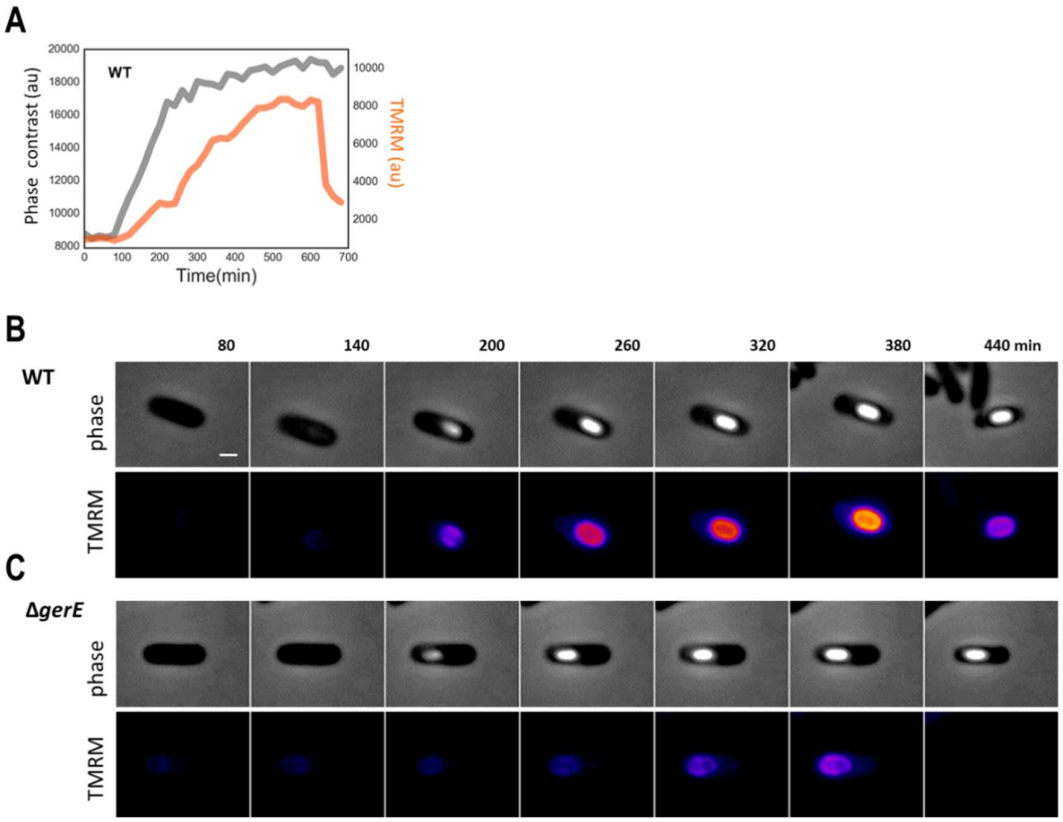

Figure S4. TMRM shows the pattern observed with ThT, Related to Figure 1
A) Time traces of phase-contrast and TMRM fluorescence in spore regions of wildtype strain. **B)** Filmstrip images of phase-contrast and TMRM fluorescence with wildtype strain. The scale bar is 1 μm. **C)** Filmstrip images of phase-contrast and TMRM fluorescence with gerE strain.

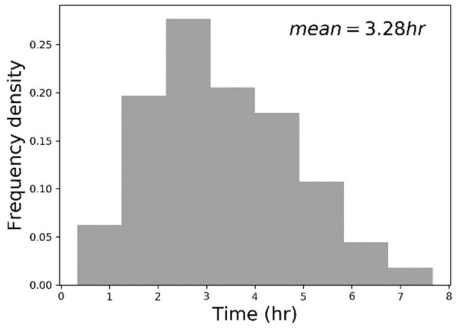

Figure S5. Histogram of the late sporulation duration in presence of ThT, Related to Figure 1
The late sporulation duration here is defined by the time between the ThT intensity reaching 1000 au and mother-cell lysis. 122 sporulating cells from two independent experiments were analyzed.

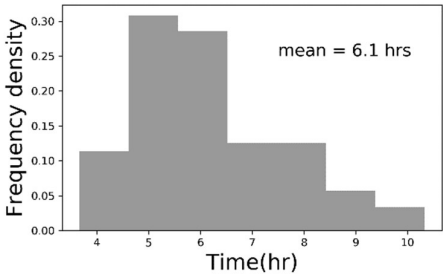

Figure S6. Histogram of the late sporulation duration in absence of ThT, Related to Figure 1
The late sporulation duration defined by the time that phase-contrast intensity started to increase until mother-cell lysis. 101 sporulating cells from three independent experiments were analyzed.

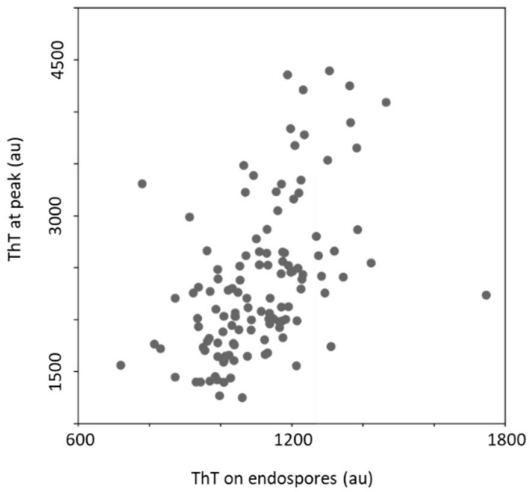

Figure S7. ThT intensity after mother-cell lysis weakly correlates with peak ThT intensity, Related to Figure 1

Scatter plot of ThT intensity after (x-axis) and before (y-axis) mother-cell lysis. The peak ThT intensity was determined by the maximum value of timeseries. 122 sporulating cells from two independent experiments were analyzed.

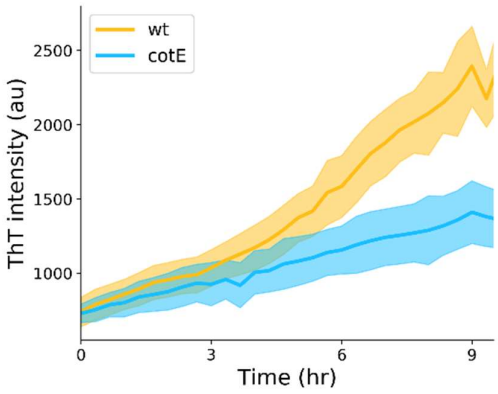

Figure S8. ThT intensity is lower in *cotE* strain, Related to Figure 2
Mean ThT time traces with wildtype and *cotE* strain. 16 wildtype cells and 34 cotE cells from two experiments were analyzed. Shaded show the standard deviations.

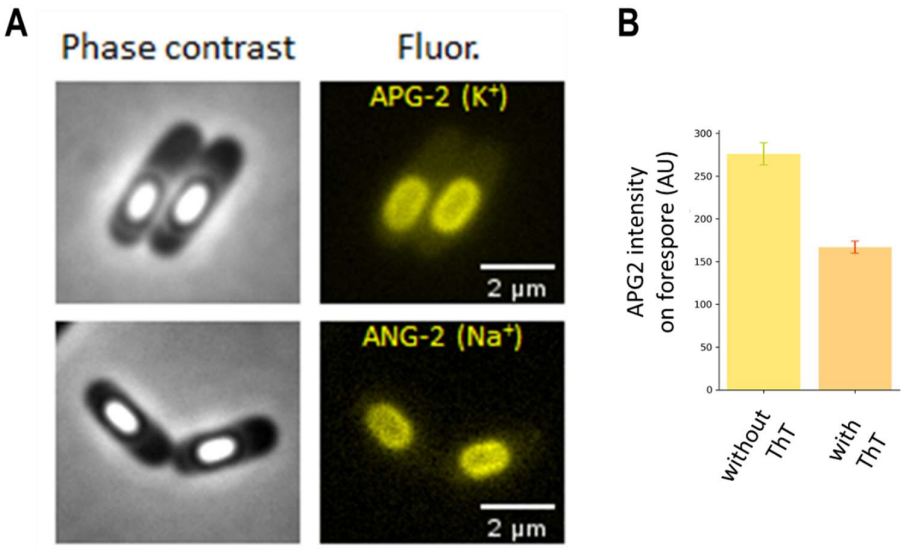

Figure S9. Potassium and sodium accumulate on forespore surfaces, Related to Figure 2
A) Microscopy images show phase contrast (left, grey), and APG2-AM and ANG2-AM fluorescence (right, yellow) on spores. Scale bar, 2 µm.
B) Quantification of APG2-AM fluorescence on forespore with and without ThT. 30 sporulating cells from three independent experiments were analyzed for each condition. Error bars are standard error of mean.

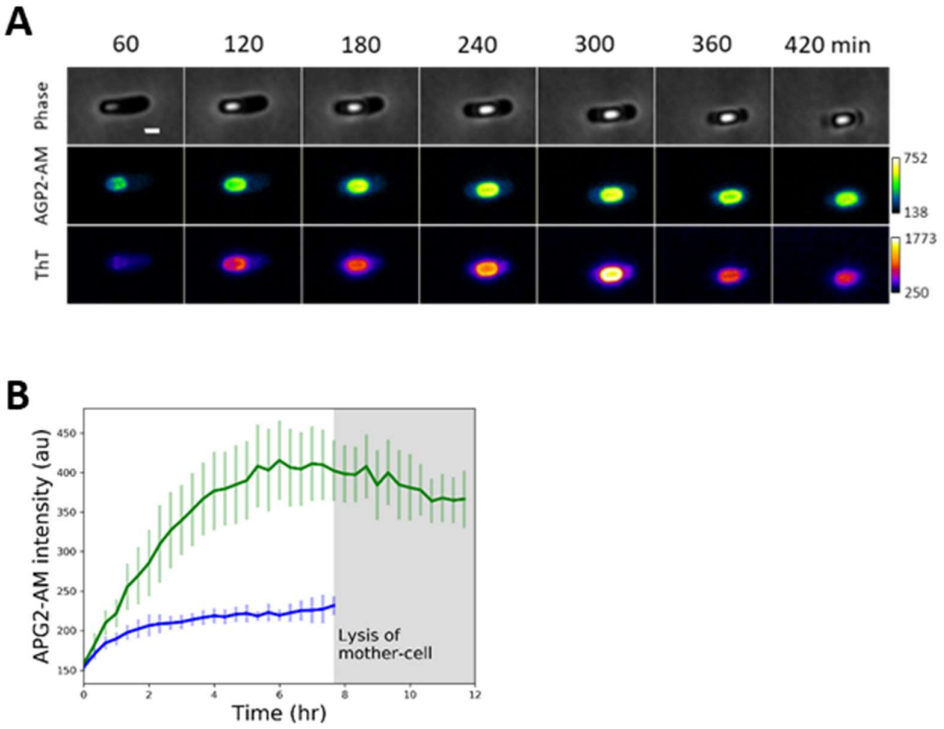

Figure S10. APG2 fluorescence increases on the forespore periphery during sporulation, Related to Figure 2

A) Phase-contrast, APG-2, ThT fluorescence images. Scale bar, 1 μm. B) Time traces of mean fluorescence intensity of APG-2 AM on the forespore regions (green, n = 14) and mother-cell cytosol (blue, n = 10). Post lysis of the mother cell signal is indistinguishable from the background. Error bars are standard deviation.

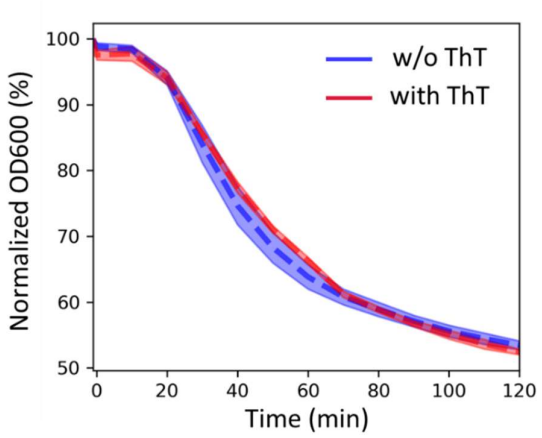

Figure S11. Germination is not affected by ThT, Related to Figure 3
Endospore germination was measured by OD600 after addition of L-alanine with and without ThT (10 μM). Shaded regions are standard deviation. Data obtained with three biological replicas.

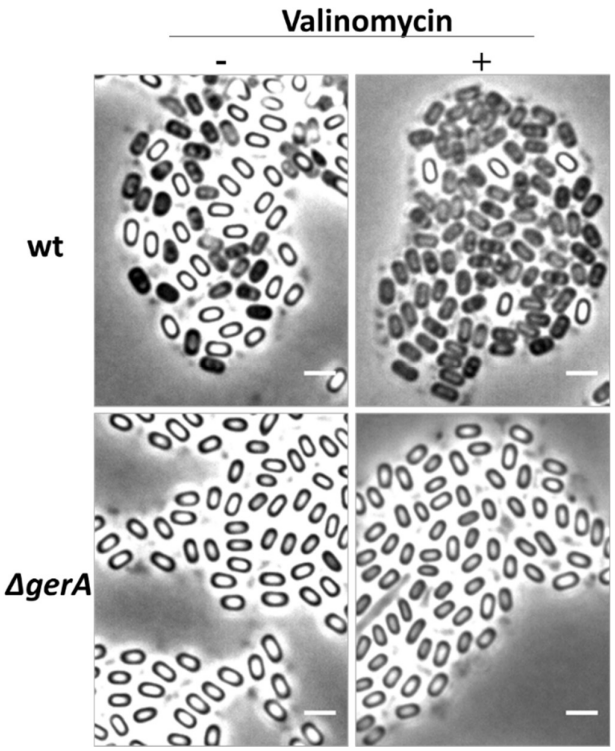

Figure S12. Valinomycin affects sporulation of wild type strain but not of *gerA* mutant, Related to Figure 4

Microscopy images showing representative samples of wild type and *gerA* mutant strain. Phase contrast (grey) images show the proportion of white and black spores without and with valinomycin treatment. Scale bar, 2 μm.

Supplementary movie legends

Movie 1. Dynamics of ThT during sporulation, Related to Figure 1
Fluorescence time-lapse microscopy images corresponding to the main Figure 1B and 1C.

Movie 2. pHluorin dynamics during sporulation, Related to Figure 1
Time-lapse microscopy images showing a sporulating cell in phase contrast (left) and pHluorin (right). The intensity in pHluorin images is the ratio of Ex466/Ex400. Lighter colors indicate low pH and darker colors indicate high pH.

Movie 3. TMRM dynamics during sporulation, Related to Figure 1
Time-lapse microscopy images of a sporulating cell in phase contrast and TMRM fluorescence.

Movie 4. Phase contrast images of live wildtype cells during sporulation, Related to Figure 3
Time-lapse microscopy showing sporulating wildtype cells in phase contrast. Several developing forespores turn phase-dark in the mother cells. Scale bar, 2 µm.

Movie 5. Phase contrast images of *gerA* cells during sporulation, Related to Figure 3
Time-lapse microscopy showing *gerA* sporulating cells in phase contrast. No premature germination was observed with this strain. Scale bar, 2 µm.

Transparent Methods

Growth Conditions and Strain Constructions

The strains of *B. subtilis* and *E. coli* used in this study are listed in Table. All strains were routinely grown in Lysogeny Broth (LB) or LB agar plates at 37 °C. When culturing the strains carrying antibiotic-resistance genes, appropriate antibiotics were supplemented in LB at the concentrations of 100 µg/mL ampicillin, 300 µg/mL spectinomycin, or 5 µg/mL chloramphenicol. All strains and primers used in this study are listed in the Table S1. PY79 *ΔgerA* strain was derived by transforming pTS39 plasmid using the standard one-step *B. subtilis* transformation procedure described previously (Jarmer et al., 2002). For the construction of pTS39 plasmid, the upstream and downstream regions of *gerAA* gene locus are amplified by Polymerase Chain Reaction (PCR) with PrimeSTAR Max DNA Polymerase (Takara) using the primer sets AP233/AP234 and AP237/AP238, respectively. The sequences of these primers, as well as all the other primers used in this study, are listed in Table. The plasmid backbone and spectinomycin-resistance cassette were amplified from pDL30 plasmid (Kuchina et al., 2011) with the primer set AP232/AP239 and AP235/AP236. The PCR products were analyzed by electrophoresis and subsequently purified from agarose gel using gel extraction kit (QIAGEN). The purified DNA fragments were then assembled using the Gibson assembly kit (NEB) and transformed into chemically competent *E. coli* cells (Top10) using the standard heat-shock transformation method. Cells were then plated onto LB agar plates with ampicillin and cultured overnight at 37°C. The colonies obtained were screened by colony PCR using the primer sets AP233/AP238. The plasmids were then extracted from the positive clones and sent for the Sanger sequencing service by the Source BioScience. The resultant sequence data were aligned to the sequence assembly *in silico* using Benchling (benchling.com). Once the sequence is confirmed, pTS39 plasmid was linearized with the restriction enzyme ScaI, and transformed into wildtype PY79. The colonies grown on LB agar plate with spectinomycin were screened by colony PCR using the primer sets AP252/AP149 and AP253/AP3 to check the double crossover homologous recombination. The positive clones were stored in 25 % glycerol at -80 °C.

Time-lapse microscopy of sporulation with Resuspension medium (RM)

The sporulation dynamics of *B. subtilis* cells were observed as previously described (Kuchina et al., 2011), using the fluorescence microscopy Leica DMi8 equipped with an automated stage, Hamamatsu Orca-flash 4.0 scientific CMOS (complementary metal–oxide–semiconductor) camera, and a PeCon incubation system. The objective lens HCX PL FLUOTAR 100x/1.30 OIL PH3 was used for all microscopy assays. ThT fluorescence was detected with 100 ms exposure with Ex438/24 and Em483/32 filters (Semrock). TMRM fluorescence was detected with 300 ms exposure with Ex554/23 and Em609/54 filters (Semrock). APG-2 and ANG-2 were detected with 300 ms exposure with Ex509/22 and Em544/22 filters (Semrock). pHluorin was detected with 300 ms exposure with Ex400/40, Ex466/40 and Em500/24 filters (Semrock). For all experiments, white LED of SOLA-SM II light engine (Lumencor) was used with the power level 10/255 (~4% of full power). For time-lapse microscopy experiments, images were taken every 20 min. For preparation of samples, overnight LB cultures of *B. subtilis* were resuspended in 20 % (v/v) LB at OD_{600} ~ 0.1 and incubated at 37 °C with shaking until reaching OD_{600} 0.6 - 0.8. The cultures were then centrifuged at 4,000 rpm (revolutions per minute) for 10 minutes, and resuspended in equal volume of pre-warmed Resuspension Medium (RM) (Sterlini and Mandelstam, 1969) (RM; composition per 1 liter: 46 µg FeCl2, 4.8 g MgSO4, 12.6 mg MnCl2, 535 mg NH4Cl, 106 mg Na2SO4, 68 mg KH2PO4, 96.5 mg NH4NO3, 219 mg CaCl2, 2 g monosodium L-glutamate), and then incubated for 3 hours at 37°C in a shaking incubator prior to microscopy assay. The cultures were then deposited on LMP (Low Melting Point) agarose pads prepared as described previously (Kuchina et al., 2011). Briefly, 1.8% (weight/volume) LMP agarose was dissolved in RM without glutamate by microwave and left to cool down before adding glutamate. When specified, fluorescent dyes or inhibitors are supplemented to the RM at the following concentrations; 1 µM APG-2 AM (TefLab), 10 µM (unless specified otherwise in the figure legend) Thioflavin T (Sigma-Aldrich), 10 µM valinomycin (Sigma-Aldrich), 20 nM TMRM (Molecular Probes). Working concentrations of these chemicals are determined based on the previous literature (Depauw et al., 2016; Kralj et al., 2011; Prindle et al., 2015; Roder and Hille, 2014). 1 mL of the RM-LMP agarose solution was placed onto a cover glass (22 millimeters by 22 millimeters) and covered by another cover glass of the same

size. Once agarose is polymerized, the coverslip on the top was removed, and 2 µL of cell cultures were deposited onto the agarose pads. The pads were cut and placed in a glass-bottom dish (Willco, HBST-5040) to be used for microscopy assays.

Spore preparation

Sporulation of *B. subtilis* cells was induced by the resuspension method of Sterlini & Mandelstam as described previously (Sterlini and Mandelstam, 1969). A single colony of *B. subtilis* was inoculated in 5 mL LB and incubated for an overnight at 37°C in a shaking incubator (200 rpm). The culture was then diluted to OD_{600} of 0.1 and incubated at 37°C in prewarmed 20% (volume/volume) LB for 3 hours to reach OD_{600} of 0.6 – 0.8. The culture was centrifuged for 10 minutes at 4,000 rpm at room temperature (RT) and resuspended in an equal volume of pre-warmed Resuspension Media (RM). After an overnight incubation in RM at 37°C in a shaking incubator, the culture was centrifuged for 10 minutes at 4,000 rpm and washed 3 times in distilled water. To remove the vegetative cells from the solution, the culture was treated with 100 µg/mL lysozyme in 10mM Tris-HCl (pH 6.8) and incubated for an hour at 37°C with aeration (200 rpm). The resultant solution was subsequently washed in 1M NaCl, milli-Q water, 1M KCl and 10 times in milli-Q water. All the centrifugation steps for washing were performed for 10 minutes at 4,000 rpm at RT. To ensure endospores are purified, the resultant solutions were inspected under microscope using 1.8% (w/v) low-melting-point agarose pad containing PBS. Spores are kept at 4°C and experiments were conducted within a week of spore preparation.

Germination assays

For the germination assay by a spectrophotometer, purified free spores were diluted to OD of ~0.8 in 1 mL sterile milli-Q water with various concentrations of salts as specified in the figure legends. The germination assays were conducted without heat shock treatments commonly used in germination assay. L-alanine was added to the final concentration of 5mM and OD_{600} was monitored using a spectrophotometer (JENWAY 7305) every 10 min for 120 min. The germination efficiencies (%) in various salt conditions were calculated as the percentage drops in OD_{600} as; $100 \times (1 - \frac{OD_{600}(t)}{OD_{600}(t_0)})$. To examine the impacts of salt to germination efficiency, the data of the last time point (t_{120}) was plotted as a function of salt concentrations.

Effects of ThT to sporulation in liquid RM

Liquid sporulating cultures in RM were prepared in the same manner described above in the section for the spore preparation. After 3.5 hours of incubation in RM, the cultures were supplemented with the final concentrations of 0 µM, 1 µM, 10 µM or 50 µM ThT and incubated at 37°C overnight in a shaking incubator (200 rpm). The cultures were then examined under microscope using LMP-agarose pads. Binary images were made for phase-bright spores and the number of phase-bright spores was determined by the particle analyzer function in imageJ (https://imagej.net/Particle_Analysis).

Wet-heat resistance assay

The spores were prepared as described above in the spore preparation section. Spore suspensions at OD600 ~1.0 were prepared and incubated at 80°C for 30 minutes (heat treatment). The samples were serially diluted and plated onto LB plates (1.5% agar) with three replica plates for each condition and serial dilution. After an overnight incubation in a 37 °C incubator, colonies on LB plates were counted, and the average values of three replica plates were used for analysis. The numbers of colonies appeared with heat-treated samples were divided by the number of colonies appeared with non-heat-treated samples to calculate the survival rate. We also performed time-lapse microscopy assay with the endospores on LB agar pads and quantified the number of endospores that outgrew in 2 hours at 37°C. Data was obtained from three biological replicates with spores prepared each time on different days.

Mathematical model

We model the dynamics of the cytoplasmic and forespore-bound cations with the following coupled differential equations:

$$\frac{dC_c}{dt} = k_2 E - k_{-2}(C_c - E) - k_1 C_c + k_{-1} C_f$$

$$\frac{dC_f}{dt} = k_1 C_c - k_{-1} C_f$$

where C_c is the concentration of cytoplasmic cations, C_f is the concentration of cations bound to forespore and E is the extracellular concentration. We define the following reactions rates:

k_1 : association constant of the cytoplasmic cations to the forespore
k_{-1} : unbinding constant of the cytoplasmic cations to the forespore
k_2 : import rate of the cation pump
k_{-2} : diffusion rate of the cation channel

Considering the development of forespore and increase with time in its negative charge, we assume that k_1 grows monotonically with time. We assume this time dependence as:

$$k_1(t) = \frac{k_{1max} t}{t_m + t}$$

This equation implies that k_1 grows and eventually saturates to a value k_{1max}, and t_m represents the time at which the crossover from linear to zero-order behavior occurs.

Given the lack of quantitative *in vivo* measurements in the literature, we chose to build a phenomenological model in which the values of the parameters are to be interpreted relative to each other, rather than in absolute quantitative terms. Our specific choice of parameter values was made to account for our experimental observations, including forespore-bound potassium and cytoplasmic potassium dynamics during sporulation. For the sake of simplicity, we neglected the potential effect of valinomycin on the active transport term parameterized by k_{-2} and ignored the potential saturation in this term as well, which does not s qualitatively change the results. The parameters used in numerical simulations are $t_m = 1$, $k_2 = 25$, $E = 5$, $k_{-1} = 0.1$, and the simulations were performed using Python.

Image analysis

The time-lapse microscopy images were analyzed with Fiji/ImageJ (National Institutes of Health) (Schindelin et al., 2012). The fore-/endo- spore regions of sporulating cells on each frame of time-lapse microscopy images were manually registered using the ROI (region of interest) manager function in ImageJ. The centroid coordinates, frame and mean pixel intensity values were measured for each ROI using the measure function in ImageJ. Obtained data sets were linked for individual cells based on the coordinate using Trackpy (github.com/soft-matter/trackpy), a Python package for particle tracking. The fluorescence intensities for individual cells were plotted. For the quantification of ThT fluorescence on endospores, a bespoke imageJ macro was developed to threshold the regions of spores based on the brightness in phase-contrast channel. ROIs were registered from the binary images and mean pixel intensities in fluorescence channel were measured for analysis. For the quantification of premature germination, phase-bright and phase-dark spores were counted at frame 30 (10 hours into time-lapse microscopy experiment).

For the estimated probability of premature germination, the confidence intervals were calculated by counting the number of events observed. The calculation was made by using the stats package in scipy (SciPy.org). Numpy (NumPy.org) and Pandas (Pandas.PyData.org) were used to calculate the standard statistical values (mean, standard deviations). All plots were created using the Python packages, matplotlib (github.com/matplotlib) and seaborn (github.com/mwaskom/seaborn).

SI Text: The use of cationic dyes to probe electrical polarity

The use of membrane-permeable fluorescent cationic molecules is a technique for probing membrane potentials of cells. The theory behind this method comes from the Nernst equation, which relates the membrane potential of a cell with the inner and outer concentrations of ions at thermodynamic equilibrium (no net flux of ions):

$$V_m = \frac{RT}{zF} \ln \frac{c_e}{c_i},$$

where R is the universal gas constant, T is the absolute temperature, z is the ionic charge, F is the Faraday constant, c_e and c_i are the external and internal concentrations of the ion respectively. If the ion in question is fluorescent and cationic, and has no specific binding to nucleic acids and other internal molecular structures in cells, then it can be used as a Nernstian dye, where the ratio of external and internal fluorescence follows the Nernst equation with the cell's membrane potential (Ehrenberg et al., 1988). For this study we used two such membrane-permeable cationic fluorescence dyes (ThT and TMRM), but not as probes for membrane potential. This is because the Coulomb interactions between the forespore coat and the cations in the mother-cell cytosol are significant, as can be seen by the spatial distribution of fluorescence dyes within a cell (Figure S2).

Under physiological conditions it is usually assumed that electric fields from surfaces are screened. This model comes from the Poisson-Boltzmann equations (generally referred to as the Guoy-Chapman model), where the electric potential ϕ decays exponentially at a Debye length λ_D,

$$\phi(x) = \phi_0 \exp\left(-\frac{x}{\lambda_D}\right)$$

$$\lambda_D = \sqrt{\frac{\epsilon k_B T}{2 z^2 e^2 c_0}},$$

where ϕ_0 is the potential at the surface, x is the distance from the surface, ϵ is the electric permittivity in the solution, k_B is the Boltzmann constant, T is the temperature, z is the valency of the ions, e is the fundamental charge, and c_0 is the bulk concentration of ions (Bazant et al., 2004). The Guoy-Chapman model for double layers assumes the system is in a steady state, meaning that the concentration profiles of the ions are static in time. By using physiological values, the Debye length in intracellular condition is ~ 1 nm, meaning that the electric field is screened at distances beyond a few nanometres (McLaughlin, 1989). The time scale for diffuse-charge dynamics is given by,

$$\tau_c = \frac{\lambda_D L}{D}$$

where L is the length scale of the system, and D is the diffusion coefficient for the ions (Bazant et al., 2004). By considering the size of the mother cell as a length scale (~ 1 μm) and using a diffusion coefficient typical to aqueous systems (~ 10^{-5} cm^2/sec), this results in a relaxation time to a steady state of 1 μs.

We suggest that the model of charge screening is inappropriate for forespore formation since this system is highly dynamic due to the uptake by ion channels found on the outer membrane of the forespore. Ion channels typically have rate constants of ≥ 10^6 ions/sec (Cahalan et al., 2001), hence the time scale for the ion concentration being reduced locally to the channel is at most 1 μs. This implies that the steady-state Guoy-Chapman model is inappropriate since the time scales are of similar magnitude and a model accounting for the dynamics of the ion channels would need to be developed. In order to accurately describe the electro-diffusion dynamics in sporulation, an alternative mathematical model could be developed, possibly based on the Nernst-Planck-Poisson euqations (Sokalski et al., 2003). Qualitatively, we expect the screening effect to be reduced, resulting in electrostatic forces being significant at distances further than the Debye length. This idea of extended screening length in cytoplasm is supported by experiments carried out in rat astrocytes, where electric fields were measured at micron scale distances from mitochondria in the cytosol (Tyner et al., 2007).

We observed a sudden drop of ThT or TMRM signal upon mother-cell lysis: when the external environment for the spore surface changes from mother-cell cytoplasm to external media. This can be qualitatively explained by the lower concentration of ThT/TMRM externally than inside mother cells. It is also possible that the thickness of the electric double layer becomes thinner due to less ion flux across outer membrane after mother-cell lysis.

Table S1. Resources, related to all figures.

***B. subtilis* strains**		
Strain	**Genotype**	**Source**
PY79	Wildtype	Lab collection
PY79 *ΔgerA*	*gerA*::*spec*^{R}	This study
PY79 *ΔspoIVCA*	*spoIVCA*	(Sandman et al., 1987)
PY79 *ΔgerE*	*gerE36*	(Zheng and Losick, 1990)
PY79 *ΔcotE*	*cotE*::*cm*^{R}	(Zheng et al., 1988)
PY79 *ΔcotB*	*cotB*::*spc*^{R}*(insertion)*	DB068 (Isticato et al., 2001)
PY79 *ΔcotG*	cotGH::*neoR; amyE*::*cotGstopcotH*	(Saggese et al., 2014)
PY79 *ΔcotBG*	*ΔcotGΔcotH*::*neo*^{R}*; amyE*::*cotGstopcotH*	Gift from Loredana Baccigalupi, University of Naples Federico II
PY79 *ΔcotC*	*cotC*::*spec*^{R} *(insertion)*	(Isticato et al., 2004)
PY79 *ΔcotU*	*cotU*::*neo*^{R} *(insertion)*	(Isticato et al., 2004)
PY79 pHluorin	*amyE*::P$_{hyperspank}$-pHluorin, *spec*^{R}	(Martinez et al., 2012)
***E. coli* strains**		
Strain	**Genotype**	**Source**
Top10	Wild type	Lab collection
Top10 pDL30	Carrying the plasmid pDL30	(Garsin et al., 1998; Kuchina et al., 2011)
Top10 ECE174	Carrying the plasmid ECE174	(Kuchina et al., 2011; Middleton and Hofmeister, 2004)
Top10 pTS39	Carrying the plasmid pTS39	This study

Primers		
Name	**Primer description**	**Primer sequence**
AP2	vector_GS351	GTCGCTACCATTACCAGTTGGTCTGG
AP3	amyE_3_GS54	AATGCAGTGGCTGAATCTTCTCC
AP22	ECE174_backbone_rev	TCCTTACGCGAAATACGGGCAG
AP149	cotZterm_pDL30_R	GCCTGCAGGCCTGCAAGCTTTTCCAGCTTGTGTAAACCTATTCATTGTTTTAAAAATATCTC
AP232	pDL30backbone_rev	AAAGGGCCTCGTGATACGC
AP233	gerAA_fwd	aaataggcgtatcacgaggcccttTTGGAACAAACAGAGTTTAAGGAATATATACAC
AP234	gerAA_rev	ttcgcgtaaggaaTCCGGGGATTGCATCAGG
AP235	spec_fwd	tgcaatccccggaTTCCTTACGCGAAATACG

AP236	spec_rev	aaagcagaatgagTGATCCCCCTATGCAAGG
AP237	gerAC_fwd	cataggggatcaCTCATTCTGCTTTCCAAAAG
AP238	gerAC_rev	ggtttgctccggcgcaaatgcagacATTTGTTTGCGCCTTTCG
AP239	pDL30_backbone_fwd	GTCTGCATTTGCGCCGGA
AP240	ECE174_backbone_rev	CATGTGCTGTCCTGCATTAATG
AP247	ECE174_backbone_fwd	CAGTACAATCTGCTCTGATGCC
AP252	gerA_5_int_check	CCATTTATGTATCCCTCCATAACGGT
AP253	gerA_3_int_check	GCCTGATCGCAGAAGGAAAGAC

Supplemental references

Bazant, M.Z., Thornton, K., Ajdari, A., 2004. Diffuse-charge dynamics in electrochemical systems. Phys. Rev. E - Stat. Physics, Plasmas, Fluids, Relat. Interdiscip. Top. 70, 24. https://doi.org/10.1103/PhysRevE.70.021506

Cahalan, M.D., Wulff, H., Chandy, K.G., 2001. Molecular properties and physiological roles of ion channels in the immune system. J. Clin. Immunol. 21, 235–252. https://doi.org/10.1023/A:1010958907271

Depauw, A., Dossi, E., Kumar, N., Fiorini-Debuisschert, C., Huberfeld, G., Ha-Thi, M.-H., Rouach, N., Leray, I., 2016. A Highly Selective Potassium Sensor for the Detection of Potassium in Living Tissues. Chemistry 22, 14902–14911. https://doi.org/10.1002/chem.201602209

Ehrenberg, B., Montana, V., Wei, M.D., Wuskell, J.P., Loew, L.M., 1988. Membrane potential can be determined in individual cells from the nernstian distribution of cationic dyes. Biophys. J. 53, 785–794. https://doi.org/10.1016/S0006-3495(88)83158-8

Garsin, D.A., Paskowitz, D.M., Duncan, L., Losick, R., 1998. Evidence for common sites of contact between the antisigma factor SpoIIAB and its partners SpoIIAA and the developmental transcription factor σ(F) in *Bacillus subtilis*. J. Mol. Biol. 284, 557–568. https://doi.org/10.1006/jmbi.1998.2201

Isticato, R., Cangiano, G., Tran, H.T., Ciabattini, A., Medaglini, D., Oggioni, M.R., De Felice, M., Pozzi, G., Ricca, E., 2001. Surface display of recombinant proteins on Bacillus subtilis spores. J. Bacteriol. 183, 6294–301. https://doi.org/10.1128/JB.183.21.6294

Isticato, R., Esposito, G., Zilhão, R., Nolasco, S., Cangiano, G., De Felice, M., Henriques, A.O., Ricca, E., 2004. Assembly of Multiple CotC Forms into the *Bacillus subtilis* Spore Coat. J. Bacteriol. 186, 1129–1135. https://doi.org/10.1128/JB.186.4.1129-1135.2004

Jarmer, H., Berka, R., Knudsen, S., Saxild, H.H., 2002. Transcriptome analysis documents induced competence of *Bacillus subtilis* during nitrogen limiting conditions. FEMS Microbiol. Lett. 206, 197–200.

Kralj, J.M., Hochbaum, D.R., Douglass, A.D., Cohen, A.E., 2011. Electrical spiking in *Escherichia coli* probed with a fluorescent voltage-indicating protein. Science 333, 345–8. https://doi.org/10.1126/science.1204763

Kuchina, A., Espinar, L., Çağatay, T., Balbin, A.O., Zhang, F., Alvarado, A., Garcia-Ojalvo, J., Süel, G.M., 2011. Temporal competition between differentiation programs determines cell fate choice. Mol. Syst. Biol. 7, 1–11. https://doi.org/10.1038/msb.2011.88

Martinez, K.A., Kitko, R.D., Mershon, J.P., Adcox, H.E., Malek, K.A., Berkmen, M.B., Slonczewski, J.L., 2012. Cytoplasmic pH response to acid stress in individual cells of *Escherichia coli* and *Bacillus subtilis* observed by fluorescence ratio imaging microscopy. Appl. Environ. Microbiol. 78, 3706–14. https://doi.org/10.1128/AEM.00354-12

McLaughlin, S., 1989. The Electrostatic Properties of Membranes. Annu. Rev. Biophys. Biophys. Chem. 18, 113–136. https://doi.org/10.1146/annurev.bb.18.060189.000553

Middleton, R., Hofmeister, A., 2004. New shuttle vectors for ectopic insertion of genes into *Bacillus subtilis*. Plasmid 51, 238–45. https://doi.org/10.1016/j.plasmid.2004.01.006

Prindle, A., Liu, J., Asally, M., Ly, S., Garcia-Ojalvo, J., Süel, G.M.G.M., 2015. Ion channels enable electrical communication in bacterial communities. Nature 527, 59–63. https://doi.org/10.1038/nature15709

Roder, P., Hille, C., 2014. ANG-2 for quantitative Na+ determination in living cells by time-resolved fluorescence microscopy. Photochem. Photobiol. Sci. 13, 1699–710. https://doi.org/10.1039/c4pp00061g

Saggese, A., Scamardella, V., Sirec, T., Cangiano, G., Isticato, R., Pane, F., Amoresano, A., Ricca, E., Baccigalupi, L., 2014. Antagonistic role of CotG and CotH on spore

germination and coat formation in Bacillus subtilis. PLoS One 9, 1–8. https://doi.org/10.1371/journal.pone.0104900

Sandman, K., Losick, R., Youngman, P., 1987. Genetic analysis of Bacillus subtilis spo mutations generated by Tn917-mediated insertional mutagenesis. Genetics 117, 603–617. https://doi.org/10.1128/JB.01343-06

Schindelin, J., Arganda-Carreras, I., Frise, E., Kaynig, V., Longair, M., Pietzsch, T., Preibisch, S., Rueden, C., Saalfeld, S., Schmid, B., Tinevez, J.-Y., White, D.J., Hartenstein, V., Eliceiri, K., Tomancak, P., Cardona, A., 2012. Fiji: an open-source platform for biological-image analysis. Nat. Methods 9, 676–82. https://doi.org/10.1038/nmeth.2019

Sokalski, T., Lingelfelter, P., Lewenstam, A., 2003. Numerical solution of the coupled Nernst-Planck and Poisson equations for liquid junction and ion selective membrane potentials. J. Phys. Chem. B 107, 2443–2452. https://doi.org/10.1021/jp026406a

Sterlini, J.M., Mandelstam, J., 1969. Commitment to sporulation in *Bacillus subtilis* and its relationship to development of actinomycin resistance. Biochem. J. 113, 29–37.

Tyner, K.M., Kopelman, R., Philbert, M.A., 2007. “Nanosized voltmeter” enables cellular-wide electric field mapping. Biophys. J. 93, 1163–1174. https://doi.org/10.1529/biophysj.106.092452

Zheng, L., Losick, R., 1990. Cascade regulation of spore coat gene expression in Bacillus subtilis. J. Mol. Biol. 212, 645–660. https://doi.org/10.1016/0022-2836(90)90227-D

Zheng, L.B., Donovan, W.P., Fitz-James, P.C., Losick, R., 1988. Gene encoding a morphogenic protein required in the assembly of the outer coat of the *Bacillus subtilis* endospore. Genes Dev. 2, 1047–54. https://doi.org/10.1101/gad.2.8.1047